

Forced Patterns of Sea Level Rise in the Community Earth System Model Large Ensemble From 1920 to 2100

John T. Fasullo^{1,2} , Peter R. Gent¹, and R. S. Nerem² 

¹National Center for Atmospheric Research, Boulder, CO, USA, ²Smead Aerospace Engineering Sciences, University of Colorado, Boulder, CO, USA

Key Points:

- The pattern of the simulated forced response in sea level from 1920 to 2100 is nonuniform in both space and time
- The altimeter era is a blend of the 20th C pattern when aerosols are important and 21st C pattern when greenhouse gases start to dominate
- Spatial patterns arise chiefly from geographic and depth variations in ocean heat content anomalies and the seawater expansion coefficient

Correspondence to:

J. T. Fasullo,
fasullo@ucar.edu

Citation:

Fasullo, J. T., Gent, P. R., & Nerem, R. S. (2020). Forced patterns of sea level rise in the community earth system model large ensemble from 1920 to 2100. *Journal of Geophysical Research: Oceans*, 125, e2019JC016030. <https://doi.org/10.1029/2019JC016030>

Received 26 DEC 2019

Accepted 1 MAY 2020

Accepted article online 7 MAY 2020

Abstract To provide context for observed sea level rise, the forced response (FR) in dynamic sea level (DSL) during the 20th and 21st centuries is examined in the Community Earth System Model Large Ensemble (LE). After accounting for simulation drift, which in the LE is sizable, the DSL FR is found to be complex, both in space and time. Its evolving character is suggested to arise from both the diversity and transient evolution of climate forcing agents and the slow adjustment timescales of the intermediate and deep oceans. Nonetheless, various intervals of spatially coherent change simulated for the recent past and near future are identified, and their characteristics and associated driving mechanisms are identified and discussed. The mid- to late-20th century DSL FR is characterized by an hemispherically asymmetric pattern of change, with depressed rates of rise in the northern oceans. There is also a dipole of change in the Southern Ocean caused by changes in near-surface zonal winds. Through the late 20th and early 21st centuries, a different pattern of rise emerges with elevated rates in the tropics and depressed rates at high latitudes. Zonal and interbasin variations characterize both intervals and involve the pattern and depth of anomalous ocean heat content storage and spatial contrasts in the expansion coefficient tied mainly to base state temperature, with greater rates of rise in warm regions per unit warming. The relative roles of surface flux and ocean convergence anomalies are examined.

Plain Language Summary Evolving patterns of sea level rise in the 20th and 21st centuries driven by climate forcings are revealed in climate model simulations and found to affect both our interpretation of past changes and projection of the future.

1. Introduction

Sea level rise is among the primary drivers of societal impacts of a changing climate (Hauer et al., 2016; Ketabchi et al., 2016; Neumann et al., 2015). In the global mean, it is driven by changes in ocean mass, associated mainly with melting of glaciers and ice sheets (Adhikari et al., 2016; Chambers et al., 2017; Katsman et al., 2008), and ocean thermal expansion, driven by a planetary energy imbalance that is stored mainly in the oceans (Bilbao et al., 2015; Cazenave, 2018; Exarchou et al., 2015; Fasullo & Nerem, 2016; Fasullo et al., 2016; Fasullo & Gent, 2017; Gregory et al. 2019). Associated impacts include enhanced flooding, salt water intrusion, erosion, and storm surges (Moftakhari et al., 2015; Neumann et al., 2015).

However, the rate of ocean rise is not uniform geographically. Rather, regional variations are both expected (Carson et al., 2016; Gregory et al., 2001; Kopp et al., 2015; Milne et al., 2009; Slangen et al., 2015) and observed (Aparna et al., 2012; Bromirski et al., 2011; Calafat et al., 2013; Carson et al., 2016), and these influence the severity of a broad range of impacts and alter the associated timescales of adaptation. Satellite observations during the altimeter era have now entered their 28th year, allowing for unprecedented estimation of both the global mean rate of rise and the magnitude of its spatial patterns, with accuracies in regional monthly fields on the order of 1 cm and long-term estimation of trends accurate to a fraction of a mm year⁻¹ (Nerem et al., 2010). The record reveals the existence of important structure in trends, spanning from eddy to planetary scales and doubling rates of rise in some regions while significantly moderating them in others.

Our understanding of the origins of these spatial patterns remains incomplete. Early in the altimeter era, the role of internal modes of climate variability in driving patterns of rise was recognized, particularly associated with the El Niño-Southern Oscillation (ENSO, Nerem et al., 1999; Chambers et al., 2002; Dieng et al., 2014; Han et al., 2017) and Pacific Decadal Variability (Cummins et al., 2005; Hamlington et al., 2014, 2016, 2019; Kenigson et al., 2018). As the altimeter era progressed, continued similarities between observed trends and

patterns of internal modes confirmed a strong role for internal variability (Caesar et al., 2018; Merrifield, 2011; Royston et al., 2018). However, more recent studies using climate models have demonstrated both: (1) a similarity between the patterns of change driven by external climate forcings (the so-called forced response, FR) and internal variability and (2) the ongoing emergence of the FR from the noise of internal variability (Fasullo & Nerem, 2018).

Furthering our understanding of altimeter era trends, and the tide gauge record that dates back to the 19th century, therefore relies on providing a longer-term perspective on forced changes. For instance, it is known that the 1991 eruption of Mt. Pinatubo played a significant role in perturbing Earth's energy budget and water cycle (Fasullo & Nerem, 2016), with a subsequent rapid reduction in global mean sea level followed by a gradual recovery during the 1990s (Fasullo et al., 2016). The occurrence of the eruption just prior to the beginning of the altimeter era impacted estimated low-frequency trends and acceleration in the global mean (Nerem et al., 2018). Did the eruption also significantly alter sea level trend patterns?

Moreover, large spatial and temporal variability has characterized anthropogenic climate forcings during the historical era (Hansen et al., 2011; Meyssignac et al., 2019), consisting mainly of anthropogenic aerosols, greenhouse gases, and reductions in polar stratospheric ozone. Each forcing has its own complex spatio-temporal evolution and climate effects. Is the regional sea level response to these combined forcings similarly complex or do climate processes act to result in a more uniform pattern of change? If the pattern is complex, what are the consequences for our understanding of sea level rise in the 20th century based on a tide-gauge record that is strongly biased towards the Northern Hemisphere? Do trends during the altimeter era strongly resemble those projected for the 21st century, and if not, why not?

Lastly, vital to understanding the sea level rise patterns during the altimeter era is an identification of the mechanisms of change. Regional sea level change is driven by winds and ocean circulation distributing heat content and mass changes around the oceans that vary with geographic location and depth. When modulated by gradients in the thermal expansion coefficient, which depends strongly on ocean temperature and depth, this results in complex regional patterns of sea level change. Aerosols and greenhouse gases are major forcings determining how much heat enters the climate system. Do they also influence the pattern of DSL rise? Another important question is what aspects of the patterns are likely to be simulated and projected robustly across a number of climate models, and what aspects are prone to strong model dependencies?

In this work, we explore these questions in the Community Earth System Model Version 1 (CESM, Hurrell et al., 2013) Large Ensemble (LE, Kay et al., 2015). A main motivation for using the LE is the opportunity it presents for estimating the FR, without the convoluting influence of model structural uncertainty that exists in multimodel ensemble means. Composed of 40 members spanning 1920–2100 and an extended contemporaneous preindustrial control simulation, the LE also provides a means for removing simulation drift. The methods and analysis approach are described in detail in section 2, while the basic physical influence of the spatial structure of the thermal expansion coefficient of sea water is documented in section 3. The time evolution of the zonal-mean FR is examined in section 4, and this motivates an analysis of coherent intervals of change preceding (1950–1993), during (1993–2020), and following (2020–2050) the altimeter era in section 5, where mechanisms of change are also explored. Lastly, the characteristics of trends across ocean basins, both in time and with depth, are explored in section 6. A concluding discussion of key results and their consequences for interpreting observed altimeter era trends is presented in section 7.

2. Methods

The CESM Version 1 is a coupled model with atmosphere, land, ocean, and sea ice components (Hurrell et al., 2013). Studies examining both its mean state and representation of variability have found the CESM to be among the highest scoring available climate models (e.g., Knutti et al., 2013). The atmospheric component, the Community Atmosphere Model Version 5, has a resolution of about 1° (288 longitude \times 192 latitude). The CESM ocean component is the Parallel Ocean Program Version 2 (POP) with resolution that is variable in latitude and is finer than 1° (320×384). The focus of this manuscript is on the POP field of sea surface height, the model variable SSH, which is equivalent to time-mean ocean dynamic sea level (DSL) as defined in Gregory et al. (2019) and is determined solely by ocean dynamics and density. It is important to note that the POP component is a Boussinesq model that has a constant volume. Therefore, while

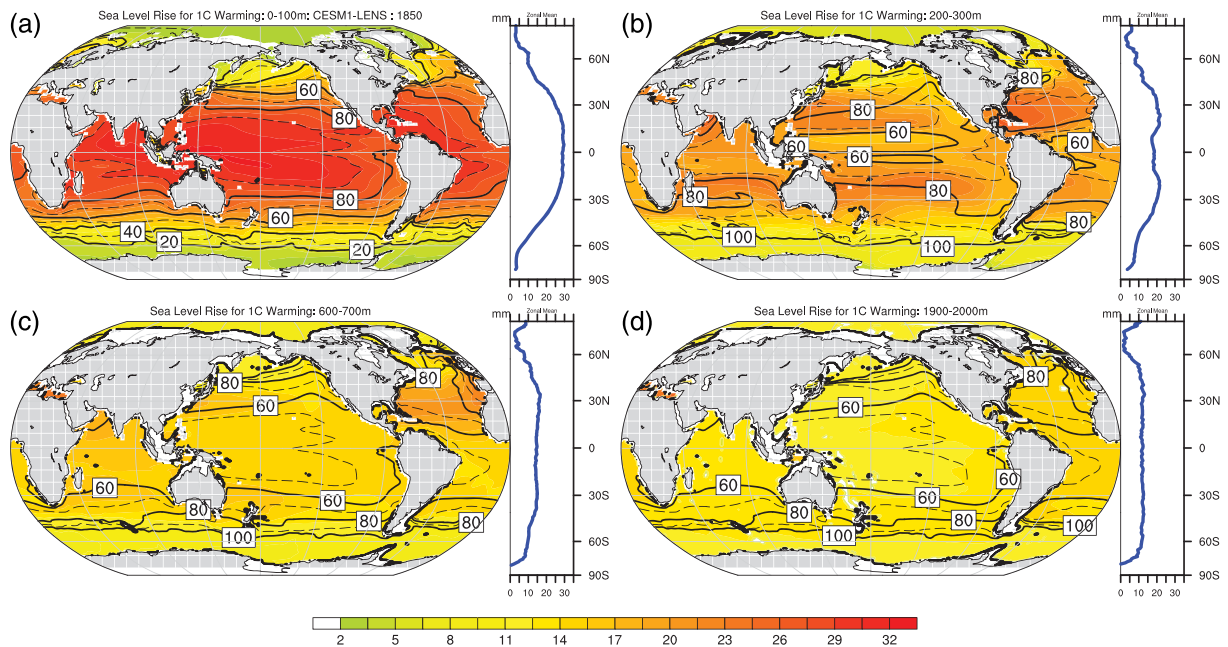


Figure 1. Estimated change in sea surface height (mm) for a 100 m deep 1°C warming across various ocean depths based on the simulated LENS 1850 control state and the equation of state (McDougall et al., 2009). Corresponding zonal means are plotted as blue lines. In (a), contour lines indicate the percent of rise relative to the western equatorial Pacific maximum. In (b–d), contour lines indicate the percent of rise relative to the 0–100 m layer amount (a) at the same latitude and longitude (at 10% intervals from 0 to 100%).

SSH fields represent the spatial patterns of sea level change, they have a constant global mean. Steric global mean sea level rise is thus not represented explicitly in POP, but can be diagnosed by postprocessing based on variations in globally averaged potential density (Greatbatch, 1994; Gregory et al., 2001). The LE initial conditions for the various ensemble members differ only in a round-off level perturbation to air temperature (Kay et al., 2015). All CESM-LE fields analyzed during this study are available on the Earth System Grid (<https://www.earthsystemgrid.org>, www.cesm.ucar.edu/projects/community-projects/LENS/). An additional 10 members of the LE that are initialized in 1920 with a broad range of initial states of the Atlantic meridional overturning circulation are also available, as described in the Appendix of Kim et al. (2018). With the exception of the first few decades in the far Southern Ocean (south of 60S), we find broad agreement between the ensemble mean in these simulations and the LE, suggesting that the choice of initialization does not exert a strong influence on our results herein. As these simulations extend only to 1999, they are not included in our broader analysis.

External climate forcing used for driving the LE include a background volcanic aerosol to minimize disruption when eruptions are prescribed as part of the historical simulations. Drift in surface temperature and other atmospheric fields is generally small. However, in the ocean, some drift remains, and this is accounted for in the analysis of section 3. A key opportunity provided by the LE is the reduction of the influence of internal variability by averaging across the ensemble, thus revealing the FR structure in both space and time. Notably, this is not readily achieved using a multimodel ensemble given the sizable structural differences in model representations of both the forced response and internal modes of variability.

Statistical significance of analyzed anomalies is gauged based on assuming interensemble spread to be Gaussian in character. Therefore, ensemble mean anomalies exceeding twice the ensemble standard error are deemed statistically significant. Values falling below this threshold are indicated by stippling where specified.

3. Sea Level Rise Sensitivity to the Location of Ocean Warming

The expansion coefficient of sea water depends strongly on temperature and pressure, and only slightly on salinity, despite having a specific heat that is approximately constant. A strong dependence therefore exists

for sea level rise as a function of where in the ocean (both geographic location and depth) changes in potential temperature occur. Based on temperature and salinity fields from preindustrial conditions in the LE, the equivalent sea level rise for a 1C increase in temperature is computed based on the POP equation of state (McDougall et al., 2009) for various depths in Figure 1. The contour lines in Figure 1a show the percentage of the rise relative to the maximum in the western equatorial Pacific, and in Figures 1b–1d, they show the percentage of rise relative to the collocated rise in the top 100 m.

Strong variations in sea level rise associated with a 1C warming are found to exist with latitude, longitude, and depth, and between basins. Near the surface (Figure 1a), rise is greatest for the warmest oceans, with a tropical maximum in the western Pacific warm pool exceeding 32 mm K^{-1} , and a tropical minimum in the eastern Pacific Ocean near 29 mm K^{-1} . Meridional variations in rise are substantial with values falling to about 50% of the tropical maximum by 50°N/S and under 20% in the polar regions. At the surface, interbasin variations are small and generally coincide with surface temperature variations. In the 200–300 m layer (Figure 1b), substantial reductions in rise are apparent, with a percentage rise that is on the order of 60 to 80% of surface values and relative minima where values fall below 60% located on the equator, where surface contributions are largest. Significant reductions in rise sensitivity relative to the surface are apparent for the 600–700 m layer (Figure 1c), where sea level contributions are generally under 20 mm K^{-1} and meridional variations are relatively weak. A notable anomalously high contribution is apparent in the North Atlantic Ocean, where strong overturning of warm, saline water contributes to increased rise. The spatial pattern of fractional rise relative to the surface is generally dominated by the structure of the surface field. Between 1.9 and 2 km (Figure 1d), values of rise are again small relative to the surface layer at most locations with the exception of polar regions, where the surface values are lower than those of the deep ocean because the deep ocean is warmer and the expansion coefficient increases with depth. Contrasts across basins are also evident with the largest values occurring in the warmer Atlantic basin.

Figure 2 shows the sea level rise for a 1C warming across a 100 m depth as a function of latitude and depth in various ocean basins. Fractional relative rates of rise relative to the surface (Figure 2a) and global ocean (Figures 2b–2e) are also shown (contour lines and intervals of 0.1). For the global ocean (Figure 2a), both strong vertical and meridional structures of rise with warming are evident with subtropical maxima extending to depth where intermediate depth overturning circulations warm deeper ocean layers and increase the coefficient of expansion. On the equator at depth contributions to rise are relatively small, due to cooler upwelling waters combined with large surface values. In polar regions, the vertical structure is the reverse, with larger values at depth than at the surface, so that ratios can exceed one. While a similar structure of rise characterizes the other ocean basins, differences are apparent nonetheless.

Particularly in the Atlantic (Figure 2b), elevated expansivity is pervasive at depth across the basin and extending to the surface in the Northern Hemisphere. Additional expansivity values of up to 0.1 to 0.2 larger than the global ocean values are apparent across large portions of the basin. In both the western and eastern Pacific Ocean (Figures 2c–2d), the reverse is true, as rise is relatively small compared to the Atlantic. Elsewhere anomalous expansivity is generally small except for the Southern Ocean, where values exceeding 0.1 exist from $50\text{--}60\text{S}$. In the Indian Ocean (Figure 2e), expansivity values elevated by 0.1 over the global ocean value exist in the Northern Hemisphere from 200–1,000 m. These regional variations in thermal expansion are driven by contrasts in the expansion coefficient as a function of temperature and depth (Figure 2f), which exhibit a strong thermal dependence and a weaker, though nonnegligible, dependence on salinity.

4. The Zonal Mean Forced Response

Given the slow timescales that characterize the ocean's response to external climate forcing, complex spatio-temporal structures often characterize its transient climate response (Smith et al., 2015; Thompson et al., 2016). Therefore, zonal-mean summaries can be useful for simplifying associated structures and identifying regimes of coherent change. As previously discussed however, an important first step in evaluating the simulated FR involves accounting for simulation drift, particularly in cases where the drift is comparable in magnitude to the FR or spatially correlated with it. Simulation drift is ubiquitous in coupled climate projections given the long timescale and associated computational challenges of reaching equilibrium in the intermediate and deeper ocean (Caesar et al., 2018; Gupta et al., 2013; Hobbs, 2016). This is true even in

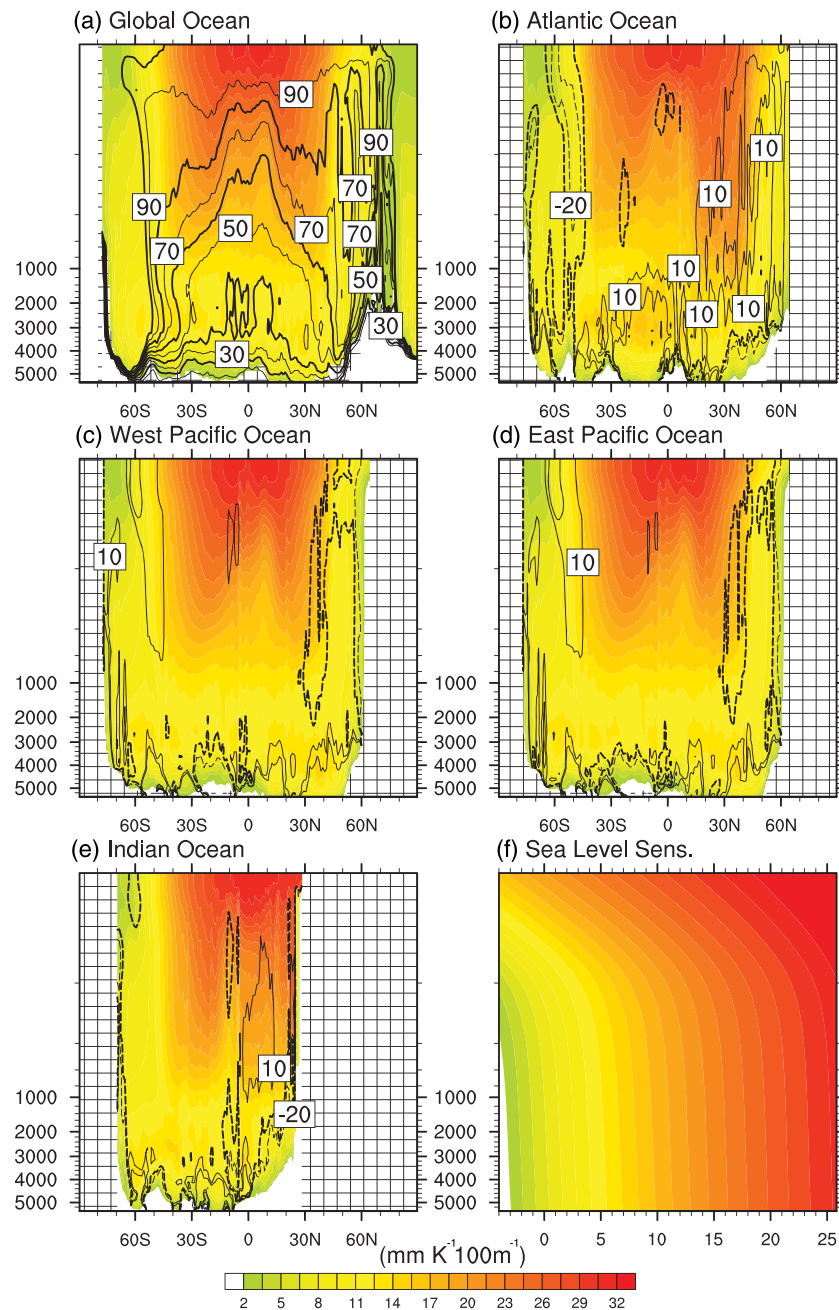


Figure 2. Estimated change in zonal-mean sea level for a uniform 1C warming across a 100 m layer ($\text{mm K}^{-1} 100 \text{ m}^{-1}$) at various depths and longitudes averaged across different ocean basins (a-Global, b-Atlantic, c-West Pacific, d-East Pacific, e-Indian) based on the LE 1850 control state. Also shown in (f) is the broader relationship between estimated rise sensitivity ($\text{mm K}^{-1} 100 \text{ m}^{-1}$), temperature (C, abscissa), and depth (i.e., pressure, ordinate) assuming salinity of 35 PSU. Contour lines in (a) depict the percent change in rise relative to the co-located surface layer (at 10% intervals from 0 to 100%) and in (b–e) represent the percent change relative to the global ocean at the same latitude and depth (at 10% intervals from -100 to 100% and dashed where negative).

the case of the LE where background volcanic aerosol have been specified in order to minimize spurious transitions in radiative forcing.

Figure 3 shows estimated DSL drift, derived from the preindustrial control simulation using a 70-year running mean applied to the zonal average at each latitude, to minimize the influence of internal variability. The average of the first 60 years has been subtracted to highlight anomalies. This drift can be easily

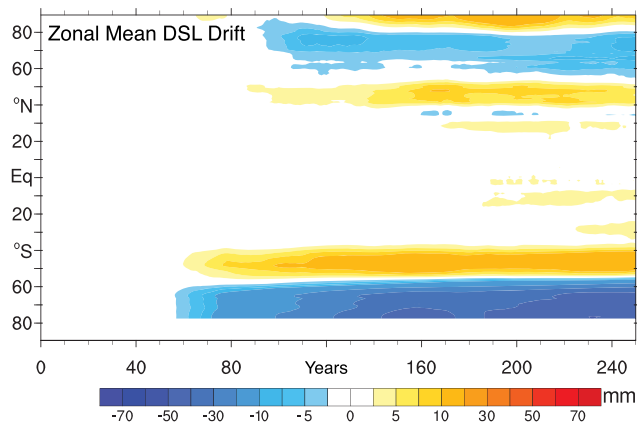


Figure 3. Zonal mean evolution of DSL (mm) in the pre-industrial control simulation (i.e., drift) for years (abscissa) that overlap with the contemporaneous 1850–2100 period in the CESM-LE (i.e., year 70 corresponds to year 1920 in the LE transient historical-era simulations). A centered 70-year running mean smoothing has been applied to reduce the influence of internal variability.

conflated with the FR, given the similarity in their magnitudes and patterns (shown below for the FR), and therefore needs to be accounted for. The drift is characterized by a dipole of DSL trends in the Southern Ocean, with negative trends south of 55S and positive trends from 40–55S, that reach almost ± 5 cm in magnitude by year 250, concurrent with year 2100 of the LE transient simulations (the first member of which starts in 1850). At other latitudes drift is smaller than in the Southern Ocean, with values near ± 1 cm in the polar and midlatitude northern oceans, and less than 0.5 cm elsewhere. Before computing the FR, the estimated drift, shown in Figure 3, is removed from each simulation member.

The FR is then calculated as the ensemble mean of the 40 member LE differenced from the smoothed control simulation. Prior to 1920, only a single member exists in the LE, and anomalies in the zonal mean are generally reflective of internal variability, with perhaps the suggestion of a response to major volcanic eruptions in the late 19th and early 20th centuries. After 1920, variability in zonal mean DSL (Figure 4a) is significantly reduced, as the internal variability contained in individual ensemble members is strongly diminished in the multi-member mean. Persisting negative anomalies in the 1920's

exist mainly in the Northern Hemisphere and are consistent with being caused by the residual effects of preceding volcanic eruptions, which generally occurred in the Northern Hemisphere and are known to cool the ocean (e.g., Fasullo et al., 2016, 2017). A concurrent dipole of anomalies is also apparent in the Southern Ocean, with an origin that is unclear. In the mid-20th century, negative anomalies in the Northern Hemisphere intensify up to the beginning of the altimeter era in 1993. In the Southern Hemisphere, after initially becoming uniformly positive briefly in the late 1960s, a dipole resembling the drift emerges and then intensifies (though again the effects of drift have been removed from the analysis). Negative anomalies in the mid-latitude Northern Hemisphere dissipate through the early 21st century, and transition to positive anomalies near 2050. Strong positive anomalies emerge north of 60 N during the altimeter era and intensify through the 21st century, while negative anomalies of similar magnitude and timing initially emerge south of approximately 60S, with coherent positive anomalies to their north and a boundary that migrates northward in the early 21st century. Figures 4b and 4c show the contribution to the forced DSL signal from steric effects for the full-depth ocean and the upper 700 m of the ocean. Both are very similar to the full DSL before 2050 in Figure 4a and so are consistent with expectations based on Figures 1 and 2, which show steric contributions to DSL (SDSL) and its spatial contrasts to be greatest in the upper ocean, an effect compounded by the disproportionate warming of the upper ocean in the 20th and 21st centuries (discussed below). The only latitude where there is a large difference between DSL and SDSL is between 60 and 80 N where the signals are of opposite sign. This indicates that dynamical effects associated with the barotropic circulation change are exerting an important influence in the region, per Lowe and Gregory (2006). It is also likely that additional heat is being stored deeper than 700 m, as this is a region of significant deep water formation in the Labrador Sea and the Greenland-Iceland-Norwegian Seas.

Mount Pinatubo in the Philippines had a major eruption in June 1991, which is just before the altimeter era. Would this eruption have been seen in DSL observations? One way to address this question is to ask that question from the LE, whose forcing includes the effects of volcanoes. Figure 4b shows that there are visible but small responses in the ensemble zonal mean DSL just after June 1991, with negative impulses between 20–30S, 30–50 N, and a short time later in the Arctic north of 70 N. However, these impulses are not large compared to the variability of individual members of the LE (e.g., as estimated from Figure 4a prior to 1920), and their regional effects are largely damped out after 3 years, which is only slightly longer than the time it takes for the volcanic aerosol perturbation to end (Fasullo et al., 2016). When viewed in both longitude and latitude, the regional influence of internal variability becomes larger still. Therefore, while the sea level signatures of large volcanic eruptions are observable from satellite for the global mean, the zonal mean signals are small relative to internal variability and are therefore unlikely to be observable unless the influence of internal variability can be removed.

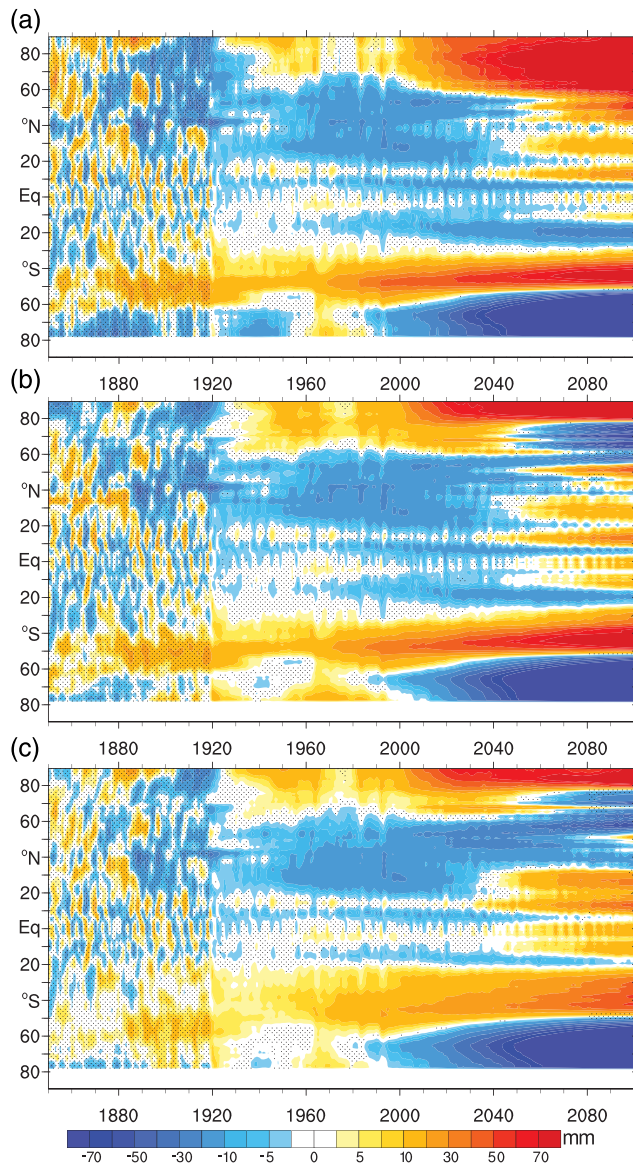


Figure 4. Zonal-mean evolution of (a) the DSL FR in the LE with the drift removed and (b) the contribution from steric effects in the full depth ocean and (c) upper 700 m of the ocean. Regions where anomalies are less than twice the ensemble standard error are stippled. Prior to 1920, only one ensemble member exists and the forced response cannot be estimated. Units of mm for all panels.

While the magnitude of all these OHC and heat convergence anomalies is statistically significant, as their magnitude exceeds twice the ensemble standard error, for some, the physical origin is unclear and will be the subject of follow-on work. Some initial insights can be gained however from consideration of the net surface shortwave (SW) component of the surface flux. Figure 7 shows the ensemble zonal mean anomalies in net downward SW flux from the LE. Comparison with the net upward heat flux in Figure 5c reveals that the decrease in SW flux into the ocean between 60 N and 40S in the mid-20th C is considerably greater than the overall decrease in F_S . Other terms in the surface energy budget act to compensate SW anomalies generally and thus SW anomalies are the basic driver of negative OHC anomalies and depressed NH DSL rise.

Figure 5a shows the zonal mean full depth ocean heat content (OHC) and Figure 5b the time rate of change of OHC from the LE. They show that the increase in OHC ramps up dramatically after 2000, and the OHC is increasing at all latitudes after 2020. However, before that time there are some signals due to the climate forcing and ocean circulation. In the Northern Hemisphere, OHC decreases at most latitudes between 1940 and 2000 in the LE. OHC between 40 and 60S starts to increase after 1960, which is likely due to the slight southward shift of the Southern Hemisphere wind maximum, which displaces the subpolar front and the core of the ACC to the south.

The rate of change of OHC (Figure 5b) shows positive and negative changes over the tropics in association with the ENSO cycle, even in the 40-member ensemble mean (after 1920) which suggests a reduced but persisting influence of internal variability. It is also plausible that high frequency variability is forced by medium sized volcanic eruptions, in 1924 and 1933, and major eruptions, in 1963, 1982, and 1991, consistent with Delworth et al. (2005). The high frequency variability is smaller generally at higher latitudes and continues throughout the RCP 8.5 scenario run. However, broader patterns are also apparent, including Northern Hemisphere cooling in the mid-20th century and after 2000 the rate of change is positive nearly everywhere, which leads to the OHC increase in Figure 5a. The cooling of the Northern Hemisphere ocean in the mid-20th century is associated with negative net downward surface flux (F_S) anomalies across a broad range of latitudes (10–70 N). Previous studies have attributed this cooling to anthropogenic aerosols (Bilbao et al., 2019; Delworth et al., 2005; Slangen et al., 2015; Tokarska et al., 2019). The increase in OHC after 2000 is a result of an increase in F_S , which is shown in Figure 5c. Other OHC features are likely driven by ocean dynamics. For example, it is notable that near the equator there is a decrease in F_S after 1950 which continues throughout the scenario up to 2100. Therefore, the increase in OHC near the equator (Figures 5a and 5b) must be driven by ocean heat convergence.

Figure 6 shows the zonal mean convergence of energy due to ocean circulation in the LE. It shows the increase in OHC along the equator after 2000 is the result of an increase in heat convergence. There is another main zone of heat convergence between 40 and 50S, and regions of increased divergence between 50 and 70 N and south of 55S. Over the 20th century, there is a region of increased divergence centered around 20S, which must be due to ocean circulation anomalies and explains the decrease in OHC centered on 20S over 1900–2000 in Figure 5a.

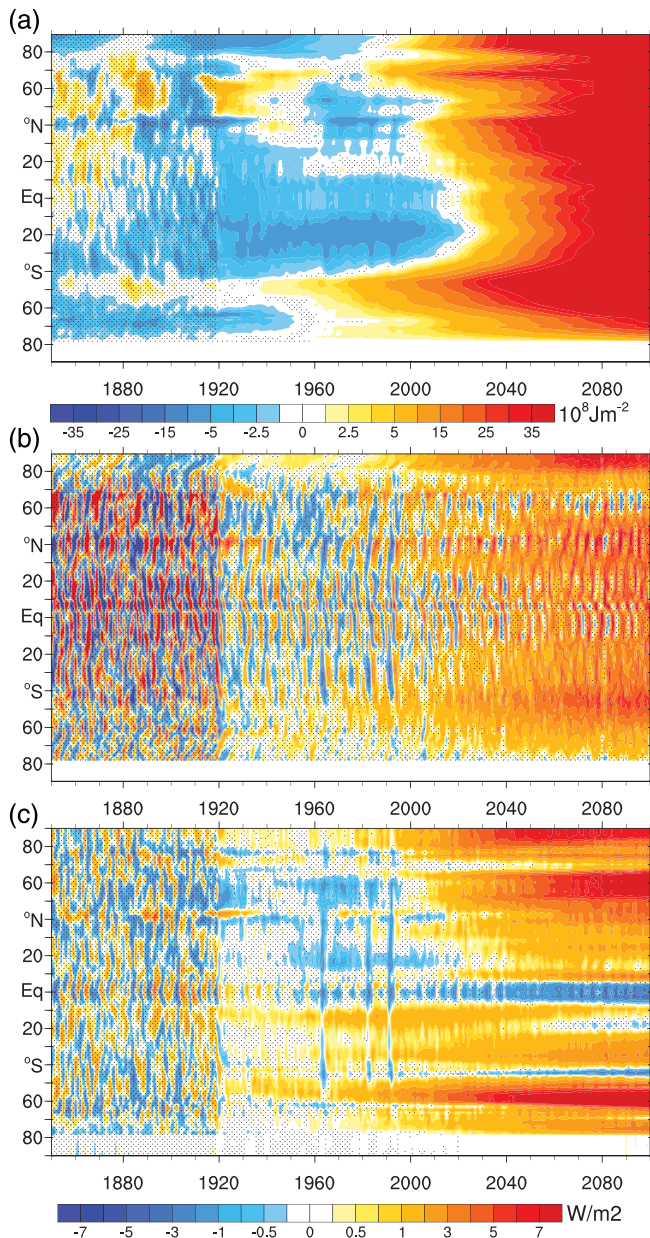


Figure 5. Zonal mean energy budget FRs associated with the evolution of DSL including (a) full-depth ocean heat content (OHC, 10^8 J m^{-2}), (b) OHC tendency (W m^{-2}), and (c) net surface heat flux (W m^{-2}).

Physically, this suggests a role for clouds and associated interactions with external climate forcing such as aerosols (Slangen et al., 2015). Future work using simulations where individual forcing agents are varied in isolation will explore these and related issues in greater detail.

5. Trend Patterns Preceding, During, and Following the Altimeter Era

Figure 8 shows the LE trends of DSL and atmospheric near-surface winds in 1950–1993, 1993–2020, and 2020–2050. These periods are chosen to represent averages of decades before, during, and after the altimeter era, and also exhibit the relative coherence in their patterns of DSL anomalies (Figure 4a). The CESM field on which DSL is based (SSH) has a global average that is zero by definition and thus does not include the globally averaged increase in ocean heat content. Figure 8a shows decreasing trends in the North Atlantic and North Pacific, which is due to decreases in ocean heat content driven by climate forcings prior to the altimeter era. In the Southern Ocean, there is a strong dipole pattern, with a band of increasing DSL to the north of a band of decreasing DSL, centered approximately about 60S. This dipole pattern is consistent with the influence of the Southern Hemisphere wind jet increasing in strength and its maximum moving slightly to the south (Armour et al. 2016). Similar wind changes have been documented in observations and can be explained by increasing levels of CO_2 and decreasing levels of stratospheric ozone over this period (Previdi & Polvani, 2014; Swart & Fyfe, 2012). These wind changes cause the ACC maximum to move slightly southward, where it is not constrained by topography, which allows the warmer water to the north of the ACC to extend further southward.

Forced responses during the altimeter era are shown in Figure 8b. DSL exhibits increases in the North Atlantic and North Pacific, reversing the negative trends from 1950–1993, while decreases span broad regions of the eastern tropical Pacific Ocean. Similar regional features are also observed during the altimeter record (e.g., Fasullo & Nerem, 2018). The dipole DSL trend in the Southern Ocean remains during 1993–2020, as also reported in Bilbao et al. (2015), although it is considerably weaker than in 1950–1993. This is consistent with the influence of a continuing increase in the strength of the zonal wind jet and a very slight southward movement of the zonal wind maximum. A similar dipole in DSL trends is also evident in the altimeter record. It is thought that the altimeter era trend has decreased compared to 1950–1993 because, although the CO_2 levels have continued to increase, the decline in stratospheric ozone has been arrested over recent decades (Marshall et al., 2014).

Figure 8c shows projected trends from the LE, which are forced by the RCP 8.5 scenario. Over this period, the forcings include a continued reduction in anthropogenic aerosols, increasing levels of CO_2 and recovery of the ozone hole in the Southern Hemisphere. The DSL trends reflect these forcings with a positive trend in the North Pacific and a continuing dipole trend in the Southern Ocean. This dipole pattern has increased in strength over 2020–2050 compared to the altimeter era because of the very strong increase in CO_2 projected in RCP 8.5. Comparison of the three panels shows that the altimeter era DSL trends are quite similar to the projected future trends, and distinct in many ways from trends during the mid-20th C. However, according to the LE results, altimeter-era DSL trends are quite representative of the DSL trends expected in the coming decade or two in many regions. The strength of these future trends will depend on the rate of future greenhouse gas emissions. If that rate is smaller than in the RCP 8.5 scenario, then the future DSL trends will likely be reduced compared to those shown in Figure 8c. In any

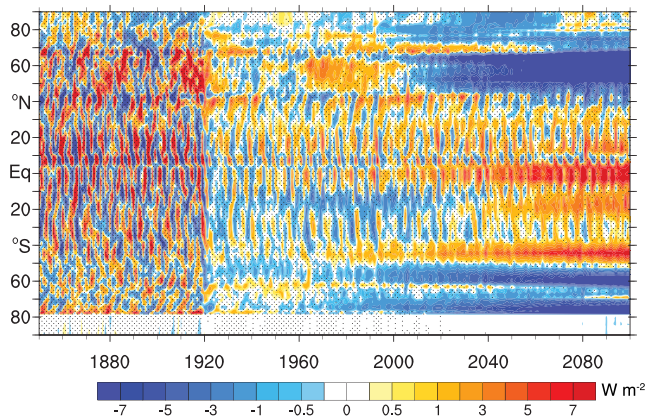


Figure 6. Inferred vertically integrated lateral ocean energy convergence (W m^{-2}) for the LE FR.

case, we can use the forced trends observed during the altimeter era as a rough indicator of what the DSL trends will look like in the near future.

6. Ocean Structure: Trends With Depth and Contrasts Across Basins

Figure 9 shows zonally averaged temperature trends in the global ocean and various basins over 1950–1993. The trends are all positive in the upper ocean and throughout the entire water column polewards of 40S and 50 N, generally consistent with climate model simulations (Bilbao et al., 2019; Tokarska et al., 2019; Figure 1). The strongest trends are in the Arctic Ocean and the Southern Ocean, especially around 50S leading to the positive band of DSL trends at that latitude shown in Figure 8a. These features are also simulated consistently in modern climate models (e.g., Slangen et al., 2015, Figure 3). Perhaps, more interesting are the negative trends near the equator from 100 m to 1 km in the Atlantic and Pacific, which continue a little deeper in the Southern Hemisphere and reach to 30S.

Figures 9e and 9f show that the Pacific cold trend is dominated by a negative trend in the west Pacific below 200 m between 20 N and 20S, whereas there is a uniform positive trend down to 300 m in the east Pacific. Figure 8a shows there are eastward trends in the zonal surface wind along the equator in the Atlantic and Pacific, which act to reduce the mean easterly zonal wind along the equator. This will reduce the amount of upwelling along the equator and the associated downwelling a few degrees off the equator. This reduction of downwelling of warm surface water will produce negative temperature trends below the upper 100–200 m. This reduction in upwelling and downwelling is stronger in the west than in the east Pacific because the mean surface easterly winds are weakest in the west and therefore reverse in sign under westerly wind trends, thereby shutting off upwelling. Therefore, these changes in upwelling and downwelling explain why there is a significant negative temperature trend below 100–200 m in the west Pacific, but a positive temperature trend in the east Pacific.

Figure 10 shows ocean temperature trends in various basins over the satellite era 1993–2020. Now the trends are positive nearly everywhere, with the only significant negative trend in the west Pacific between 10 N–10S and 150–400 m. This negative trend can again be explained by a positive trend in zonal surface wind in this region, which is shown in Figure 8b. There are still positive trends in zonal wind along the equator in the east Pacific and Atlantic, but these are now small and so do not significantly reduce the amount of upwelling. In addition, over this era there is a quite strong positive temperature trend due to the extra heat coming from the atmosphere caused by rising levels of greenhouse gases. This greenhouse gas signal is much stronger in the satellite era than it was previously from 1950–1993.

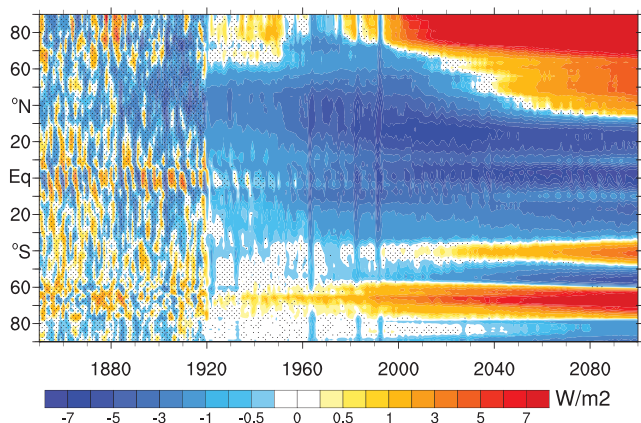


Figure 7. Zonal-mean net downward surface shortwave flux FR (W m^{-2}) for the LE. Regions where anomalies are less than twice the standard error are stippled.

Figure 11 shows the projected ocean temperature trends in the future 2020–2050. Now negative trends are confined to a very small region in the west Pacific, and again are consistent with a positive trend in the zonal surface wind (Figure 8c). However, now the large positive trends are dominated by the global warming signal as the upper ocean is receiving large amounts of extra heat due to the strongly rising level of CO_2 in the RCP 8.5 scenario. The disproportionate warming of the upper ocean, cited earlier, is an important contributor to observed patterns of DSL change. In addition, as for trends in DSL, the ocean temperature trends over the satellite era closely resemble future temperature trends and are distinct from trends over 1950–1993. Again, the magnitude of these ocean temperature trends over 2020–2050 will depend on the future rate of increase in climate forcings.

7. Discussion, Conclusions, and Future Work

The LE provides the opportunity to directly estimate the CESM's response of dynamic sea level to external climate forcings in the absence of the

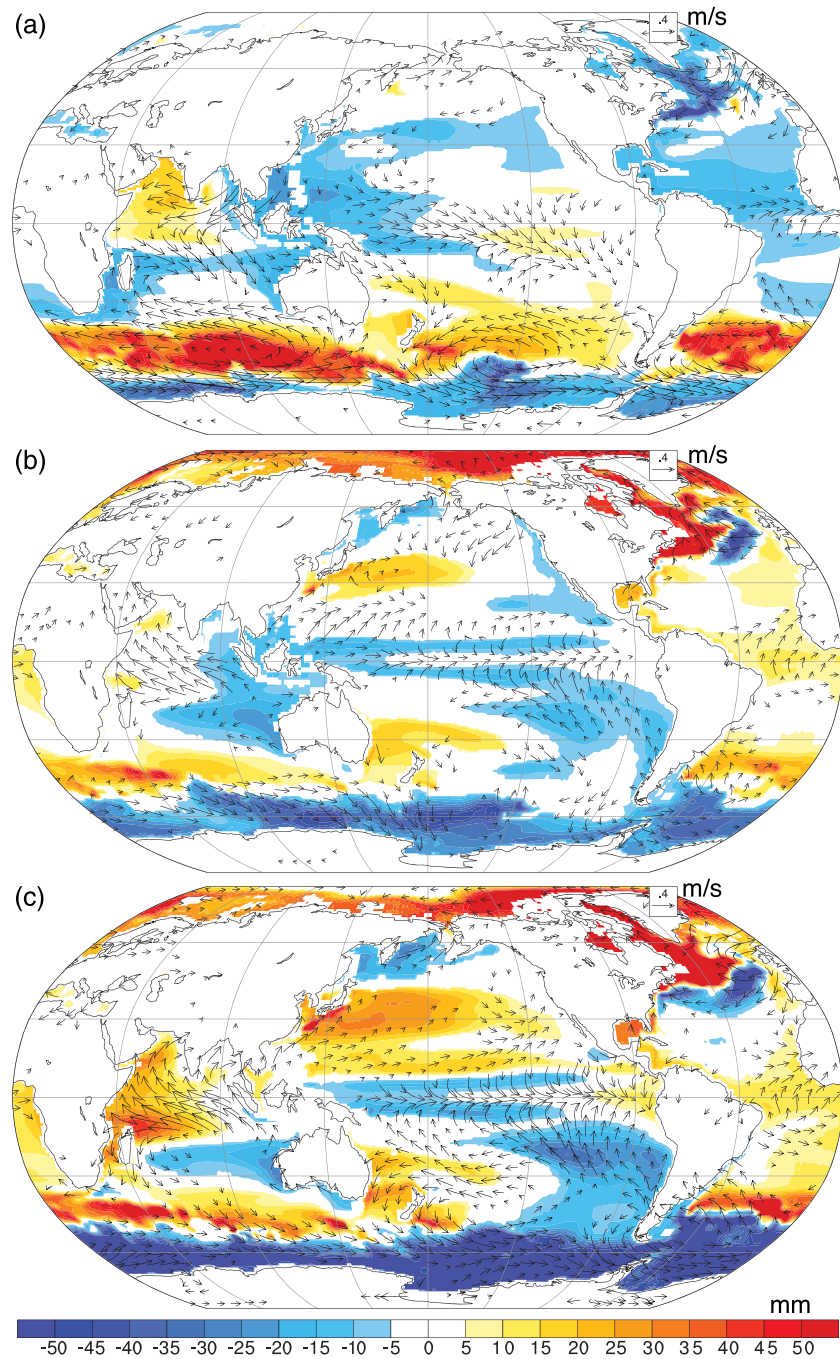


Figure 8. Total LE FR trends in DSL (filled contours, mm) and atmosphere surface winds (vectors, m s^{-1}) in (a) decades prior to (1950–1993), (b) during (1993–2020), and (c) after (2020–2050) the altimeter era. Regions of filled contours are significant based on the FR trend being more than twice the standard error.

convoluting effects of model structural uncertainty. It reveals various key aspects of regional sea level's FR to climate change. First, it demonstrates the spatial and temporal complexity of the response, which exhibits strong latitudinal variations and changes of magnitude, and even sign, through the 20th and 21st centuries. Moreover, the continually evolving pattern of the FR contrasts with the relatively constant Cazenave, 2018; pattern other surface and atmospheric fields (Lee, 2014), posing a particular challenge for attempts to characterize its transient evolution through pattern scaling approaches, at least on a global basis (Tebaldi & Arblaster, 2014). These aspects, combined with the large internal variability of regional

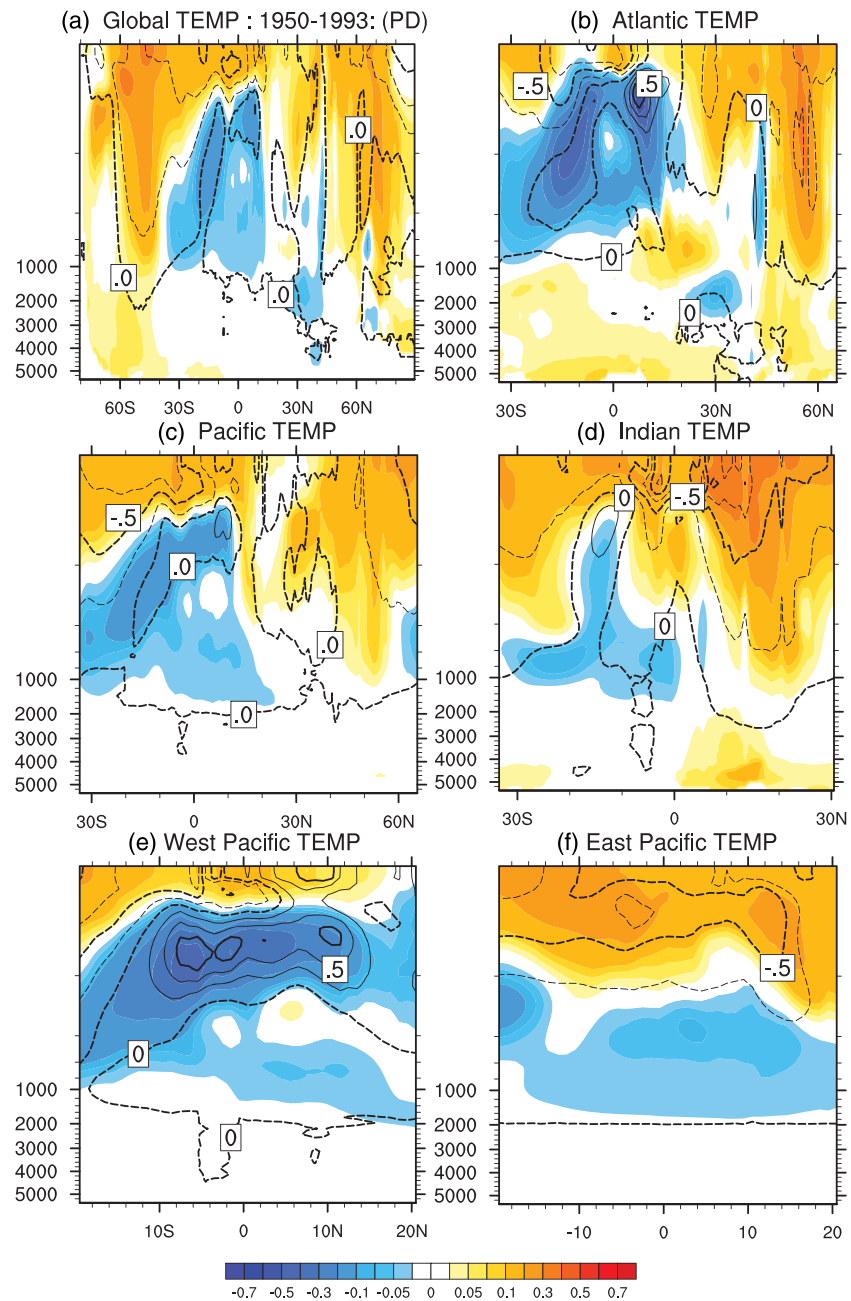


Figure 9. Zonal mean FR trends of LE zonally averaged temperature (filled contours, K) and potential density (lines, $10^{-4} \text{ g cm}^{-3}$, intervals of 0.25) in various basins for 1950–1993.

sea level and the sampling challenges of the tide gauge and altimeter records, suggest that the insight into attribution of sea level variability provided by models will be central to distinguishing between natural and anthropogenic influences.

Of particular note is the strong interhemispheric contrast in DSL in the CESM-LE during the mid-20th century and the potential significance it holds for the tide gauge record, which is located overwhelmingly in the Northern Hemisphere. As the spatial pattern of the FR has yet to be accounted for in tide gauge reconstructions, associated sampling bias and consequences for global mean estimates of rise and acceleration remain largely unknown, and will be the subject of follow-on work. Specifically, the potential for aliasing of the FR onto the observed record as an explanation for the challenges that exist in closing the 20th century sea level

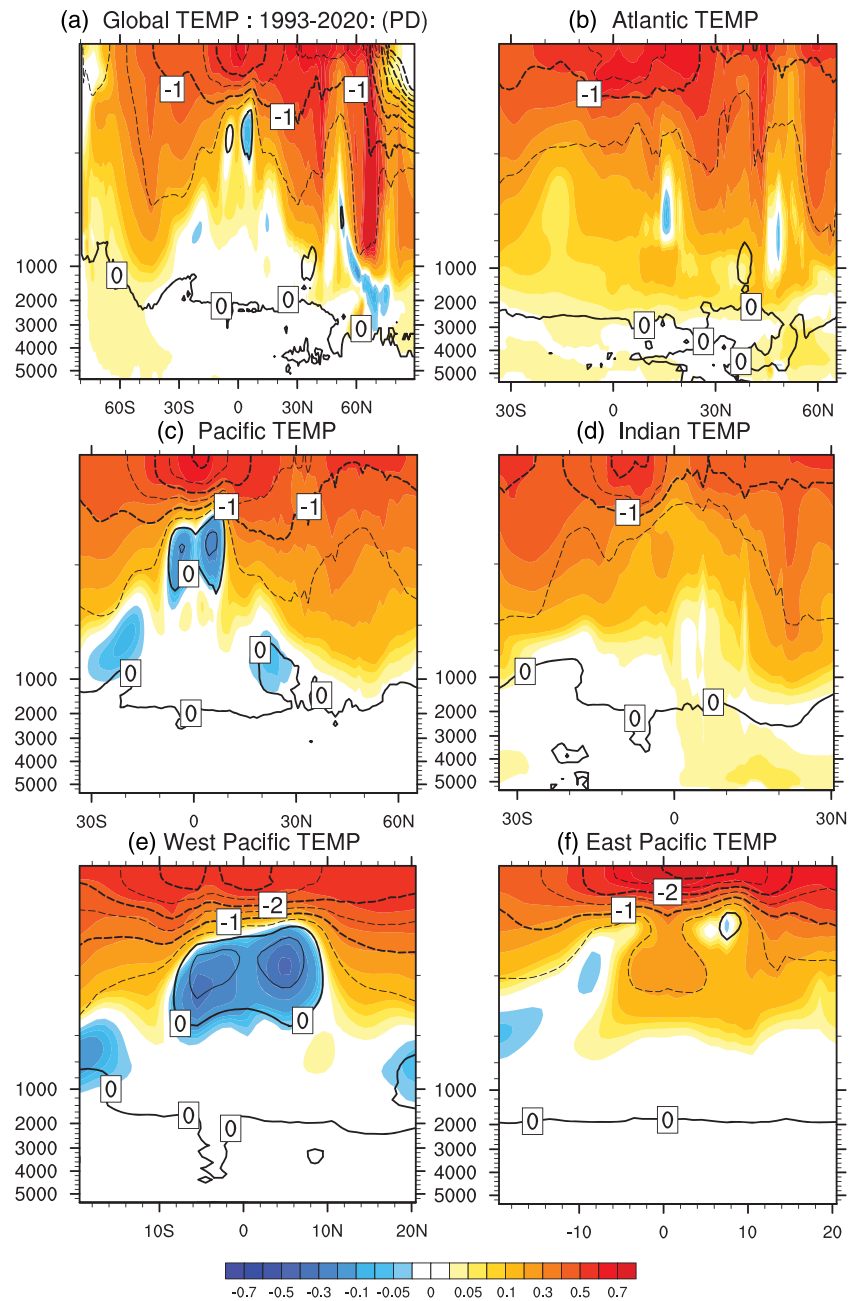


Figure 10. As in Figure 9 except for 1993–2020. Units are K (filled contours) and $10^{-4} \text{ g cm}^{-3}$. (lines, intervals of 0.5).

budget (Chambers et al., 2012; Gregory et al., 2013) remains to be explored beyond multi-model averages. Adequately addressing this and related issues mandates the use of a large ensemble with an accurate depiction of the FR, as multimodel ensembles give conflicting representations of both internal variability and forced change, resulting in multimodel averages of questionable significance (Kay et al., 2015).

The CESM-LE also highlights the relative insensitivity of regional patterns of rise to major volcanic eruptions, which while driving brief transient anomalies in DSL are largely obscured by lower frequency transient forcing of the climate system. A physical basis for this insensitivity, the relatively small OHC perturbations imposed relative to the accumulated changes driven by other climate forcings, is suggested.

There are also important implications of these insights for our interpretation of the altimeter era, which lies at the nexus of distinct patterns that characterize the mid-20th century and 21st century. While a strong

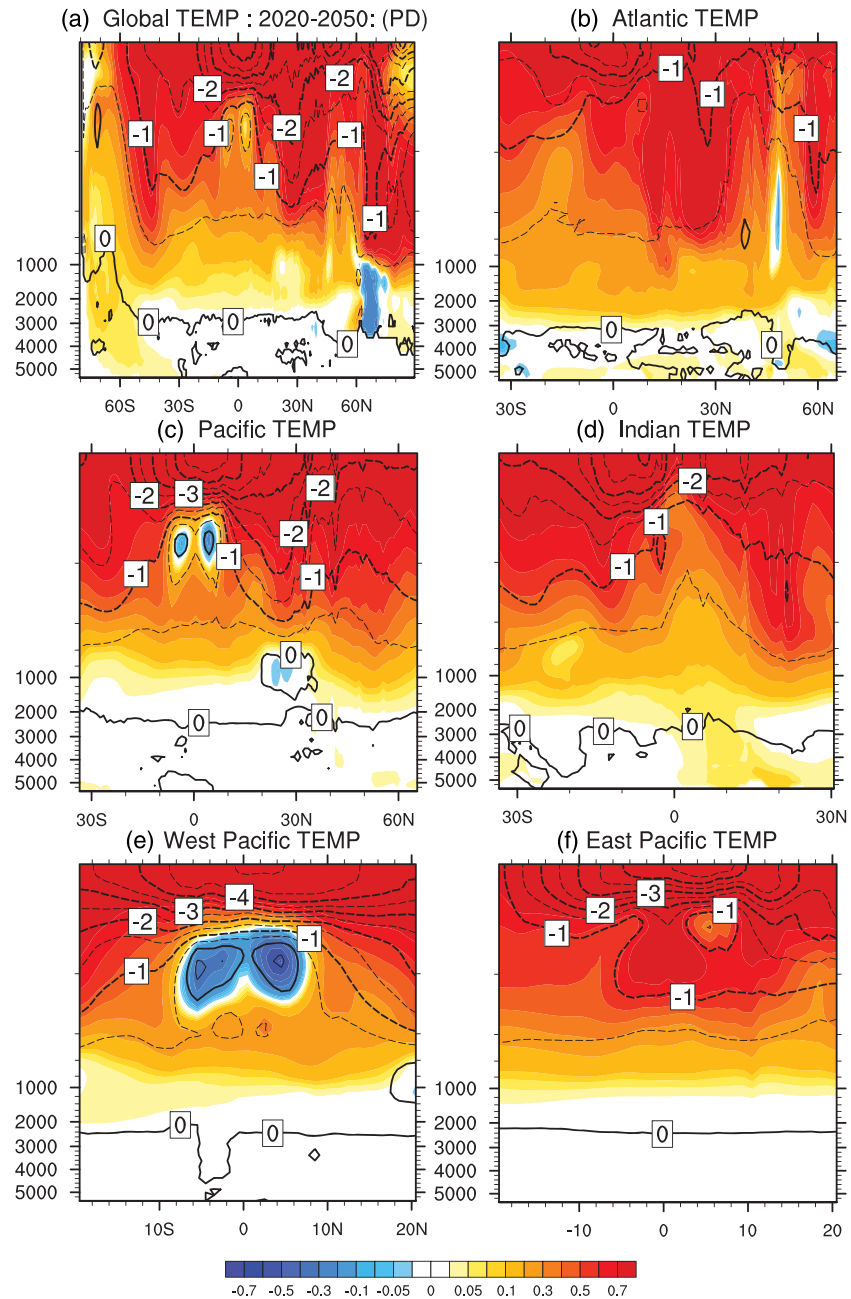


Figure 11. As in Figure 9 except for 2020–2050. Units are K (filled contours) and $10^{-4} \text{ g cm}^{-3}$. (lines, intervals of 0.5).

similarity does exist between altimeter-era and near-future trends, consistent with the conclusions of Fasullo and Nerem et al. (2018), vestiges of the 20th century pattern are evident in the altimeter record. These include, for example, the rebound in the Atlantic Ocean from depressed rates of rise in the mid-20th century, with particular significance along the eastern seaboard of North America. In some respects, the correct interpretation of 21st century patterns relies on an understanding of the 20th century, as the exceptional strength in basin-scale rates of rise in the Atlantic in the early 21st century reflect the previously depressed rates that characterized the 20th century.

An important caveat that persists is the degree to which results obtained using the CESM-LE are robust across other models and adequate depictions of nature. The CESM ocean component is low resolution, and the effects of mesoscale eddies are parameterized (Chelton et al., 2007; Gent & McWilliams, 1990).

However, Bryan et al. (2014) show that this model with parameterized eddies gives very similar ocean heat uptake results in the Southern Ocean to a version that explicitly resolves the effects of eddies. In addition, Farneti et al. (2015) conclude that the CESM ocean component is one of the best climate models simulating both eddy compensation and eddy saturation in the Southern Ocean. What role do such eddies play in regional ocean energy convergence and associated sea level trends? Additionally, it can be asked what model dependence is likely to affect the pattern of anomalous F_S and OHC accumulation? It is known that feedbacks and perturbed flows of energy through climate models depend in part upon changes in clouds and moisture that are simulated inconsistently in key respects across models. Also important, and perhaps central, is the uncertainty of interactions between clouds and climate forcings, and particularly aerosols. It remains to be seen whether the core conclusions reached here are robust to alternative choices of climate models and to what degree differences in their feedbacks and forcing interactions might affect these results. In turn, the opportunity to constrain models using the altimeter record as a measure of regional sea level and ocean heat content variability remains largely unexplored. Another caveat is that the CESM does not include interactive ice sheets, so that the response due to freshwater input from ice loss in Greenland and Antarctica, as for example discussed in Stammer (2008), Lorbacher et al. (2012), and Agarwal et al. (2014), is not included in the results presented here. If ice sheet melt continues to increase strongly in the near future, then this will have a possibly dramatic effect on the DSL projections presented here.

Lastly, while the analysis here has established ties between external climate forcing and regional sea level responses, the role of individual climate forcings remains unclear. Establishing connections between forcing and responses allows for the attribution of past changes, and in instances where the signal of response is large compared to internal noise, the evaluation of models and forcing. Separation of the influence of forcings in the future may also help guide policy as connections between forcing agents, particularly aerosols, and regional sea level responses are potentially strong. Providing a detailed accounting of such connections, and the uncertainties involved related to models and forcings as discussed above, may serve as useful guidance to policymakers in navigating the complexities of a changing climate.

Acknowledgments

This material is based upon work supported by the National Center for Atmospheric Research, which is a major facility sponsored by the National Science Foundation under Cooperative Agreement No. 1852977. The efforts of Dr. Fasullo in this work were partially supported by the Regional and Global Model Analysis (RGMA) component of the Earth and Environmental System Modeling Program of the U.S. Department of Energy's Office of Biological & Environmental Research (BER) via National Science Foundation IA 1844590. The efforts of Dr. Fasullo in this work were also supported in part by NSF Award #AGS-1419571. Additional support for the efforts of Drs. Fasullo and Nerem has been provided by NASA Award 80NSSC17K0565. Data used in this study can be obtained at <https://www.earthsystemgrid.org>. We wish to recognize the efforts of two anonymous reviewers for their thoughtful and substantive suggestions.

References

- Adhikari, S., Ivins, E. R., & Larour, E. (2016). ISSM-SESAW v1.0: Mesh-based computation of gravitationally consistent sea-level and geodetic signatures caused by cryosphere and climate driven mass change. *Geoscientific Model Development*, *9*, 1087–1109.
- Agarwal, N., Köhl, A., Mechoso, C. R., & Stammer, D. (2014). On the early response of the climate system to a meltwater input from Greenland. *Journal of Climate*, *27*(21), 8276–8296. <https://doi.org/10.1175/jcli-d-13-00762.1>
- Aparna, S. G., McCreary, J. P., Shankar, D., & Vinayachandran, P. N. (2012). Signatures of Indian Ocean Dipole and El Niño-Southern Oscillation events in sea level variations in the Bay of Bengal. *Journal of Geophysical Research*, *117*, C10012. <https://doi.org/10.1029/2012JC008055>
- Armour, K. C., Marshall, J., Scott, J. R., Donohoe, A., & Newsom, E. R. (2016). Southern Ocean warming delayed by circumpolar upwelling and equatorward transport. *Nature Geoscience*, *9*, 549–554.
- Bilbao, R. A., Gregory, J. M., & Bouttes, N. (2015). Analysis of the regional pattern of sea level change due to ocean dynamics and density change for 1993–2009 in observations and CMIP5 AOGCMs. *Climate Dynamics*, *45*, 2647–2666.
- Bilbao, R. A., Gregory, J. M., Bouttes, N., Palmer, M. D., & Stott, P. (2019). Attribution of ocean temperature change to anthropogenic and natural forcings using the temporal, vertical and geographical structure. *Climate Dynamics*, *53*(9–10), 5389–5413.
- Bromirski, P. D., Miller, A. J., Flick, R. E., & Auad, G. (2011). Dynamical suppression of sea level rise along the Pacific coast of North America: Indications for imminent acceleration. *Journal of Geophysical Research*, *116*, C07005. <https://doi.org/10.1029/2010JC006759>
- Bryan, F. O., Gent, P. R., & Tomas, R. (2014). Can Southern Ocean eddy effects be parameterized in climate models? *Journal of Climate*, *27*, 411–425.
- Caesar, L., Rahmstorf, S., Robinson, A., Feulner, G., & Saba, V. (2018). Observed fingerprint of a weakening Atlantic Ocean overturning circulation. *Nature*, *556*(7700), 191–196. <https://doi.org/10.1038/s41586-018-0006-5>
- Calafat, F. M., Chambers, D. P., & Tsimplis, M. N. (2013). Inter-annual to decadal sea-level variability in the coastal zones of the Norwegian and Siberian Seas: The role of atmospheric forcing. *Journal of Geophysical Research: Oceans*, *118*, 1287–1301. <https://doi.org/10.1002/jgrc.20106>
- Carson, M., Köhl, A., Stammer, D., Slangen, A. B. A., Katsman, C. A., van de Wal, R. S. W., et al. (2016). Coastal sea level changes, observed and projected during the 20th and 21st century. *Climatic Change*, *134*(1–2), 269–281. <https://doi.org/10.1007/s10584-015-1520-1>
- Cazenave, A. (2018). Global sea-level budget 1993–present. *Earth System Science Data*, *10*(3), 1551–1590. <https://doi.org/10.5194/essd-10-1551-2018>
- Chambers, D. P., Cazenave, A., Champollion, N., Dieng, H., Llovel, W., Forsberg, R., et al. (2017). Evaluation of the global mean sea level budget between 1993 and 2014. In *Integrative Study of the Mean Sea Level and Its Components*, (pp. 315–333). Cham: Springer. https://doi.org/10.1007/978-3-319-56490-6_14
- Chambers, D. P., Mehlhaff, C. A., Urban, T. J., Fujii, D., & Nerem, R. S. (2002). Low-frequency variations in global mean sea level: 1950–2000. *Journal of Geophysical Research*, *107*(C4), 3026. <https://doi.org/10.1029/2001JC001089>
- Chambers, D. P., Merrifield, M. A., & Nerem, R. S. (2012). Is there a 60-year oscillation in global mean sea level? *Geophysical Research Letters*, *39*, L18607. <https://doi.org/10.1029/2012GL052885>

- Chelton, D. B., Schlax, M. G., Samelson, R. M., & de Szoeke, R. A. (2007). Global observations of large oceanic eddies. *Geophysical Research Letters*, *34*, L15606. <https://doi.org/10.1029/2007GL030812>
- Cummins, P. F., Lagerloef, G. S. E., & Mitchum, G. (2005). A regional index of Northeast Pacific variability based on satellite altimeter data. *Geophysical Research Letters*, *32*, L17607. <https://doi.org/10.1029/2005GL023642>
- Delworth, T. L., Ramaswamy, V., & Stenchikov, G. L. (2005). The impact of aerosols on simulated ocean temperature and heat content in the 20th century. *Geophysical Research Letters*, *32*, L24709. <https://doi.org/10.1029/2005GL024457>
- Dieng, H. B., Cazenave, A., Meyssignac, B., Henry, O., von Schuckmann, K., Palanisamy, H., & Lemoine, J. M. (2014). Effect of La Niña on the global mean sea level and North Pacific Ocean mass over 2005–2011. *Journal of Geodetic Science*, *4*(1). <https://doi.org/10.2478/jogs-2014-0003>
- Exarchou, E., Kuhlbrodt, T., Gregory, J. M., & Smith, R. S. (2015). Ocean heat uptake processes: A model intercomparison. *Journal of Climate*, *28*, 887–908. <https://doi.org/10.1175/JCLI-D-14-00235.1>
- Farneti, R., Downes, S. M., Griffies, S. M., Marsland, S. J., Behrens, E., Bentsen, M., et al. (2015). An assessment of Antarctic Circumpolar Current and Southern Ocean Meridional Overturning Circulation during 1958–2007 in a suite of interannual CORE-II simulations. *Ocean Modelling*, *93*, 84–120. <https://doi.org/10.1016/j.ocemod.2015.07.009>
- Fasullo, J. T., & Gent, P. R. (2017). On the relationship between regional ocean heat content and sea surface height. *Journal of Climate*, *30*, 9195–9211.
- Fasullo, J. T., & Nerem, R. S. (2016). Interannual variability in global mean sea level estimated from the CESM large and last millennium ensembles. *Water*, *8*(11), 491.
- Fasullo, J. T., & Nerem, R. S. (2018). Altimeter-era emergence of the patterns of forced sea-level rise in climate models and implications for the future. *Proceedings of the National Academy of Sciences*, *115*(51), 12,944–12,949. <https://doi.org/10.1073/pnas.1813233115>
- Fasullo, J. T., Nerem, R. S., & Hamlington, B. (2016). Is the detection of accelerated sea level rise imminent? *Scientific Reports*, *6*, 31,245.
- Fasullo, J. T., Tomas, R., Stevenson, S., Otto-Bliesner, B., Brady, E., & Wahl, E. (2017). The amplifying influence of increased ocean stratification on a future year without a summer. *Nature Communications*, *8*(1), 1236. <https://doi.org/10.1038/s41467-017-01302-z>
- Gent, P. R., & McWilliams, J. C. (1990). Isopycnal mixing in ocean circulation models. *Journal of Physical Oceanography*, *20*, 150–155.
- Greatbatch, R. J. (1994). A note on the representation of steric sea level in models that conserve volume rather than mass. *Journal of Geophysical Research*, *99*, 12,767–12,771.
- Gregory, J., Church, J. A., Boer, G. J., Dixon, K. W., Flato, G. M., Jackett, D. R., et al. (2001). Comparison of results from several AOGCMs for global and regional sea-level change 1900–2100. *Climate Dynamics*, *18*(3–4), 225–240. <https://doi.org/10.1007/s003820100180>
- Gregory, J. M., Griffies, S. M., Hughes, C. W., Lowe, J. A., Church, J. A., Fukimori, I., et al. (2019). Concepts and terminology for sea level: Mean, variability and change, both local and global. *Surveys in Geophysics*, *40*, 1251–1289.
- Gregory, J. M., White, N. J., Church, J. A., Bierkens, M. F. P., Box, J. E., Van den Broeke, M. R., et al. (2013). Twentieth-century global-mean sea level rise: Is the whole greater than the sum of the parts? *Journal of Climate*, *26*(13), 4476–4499. <https://doi.org/10.1175/JCLI-D-12-00319.1>
- Gupta, A. S., Jourdain, N. C., Brown, J. N., & Monselesan, D. (2013). Climate drift in the CMIP5 models. *Journal of Climate*, *26*, 8597–8615. https://doi.org/10.1175/JCLI_D_12_00521.1
- Hamlington, B. D., Cheon, S. H., Thompson, P. R., Merrifield, M. A., Nerem, R. S., Leben, R. R., & Kim, K. Y. (2016). An ongoing shift in Pacific Ocean sea level. *Journal of Geophysical Research: Oceans*, *121*, 5084–5097. <https://doi.org/10.1002/2016JC011815>
- Hamlington, B. D., Fasullo, J. T., Nerem, R. S., Kim, K. Y., & Landerer, F. W. (2019). Uncovering the pattern of forced sea level rise in the satellite altimeter record. *Geophysical Research Letters*, *46*, 4844–4853. <https://doi.org/10.1029/2018GL081386>
- Hamlington, B. D., Strassburg, M. W., Leben, R. R., Han, W., Nerem, R. S., & Kim, K. Y. (2014). Uncovering an anthropogenic sea-level rise signal in the Pacific Ocean. *Nature Climate Change*, *4*(9), 782.
- Han, W., Meehl, G. A., Stammer, D., Hu, A., Hamlington, B. D., Kenigson, J., et al. (2017). Spatial patterns of sea level variability associated with natural internal climate modes. *Surveys in Geophysics*, *38*(1), 217–250.
- Hansen, J., Sato, M., Kharecha, P., & Von Schuckmann, K. (2011). Earth's energy imbalance and implications. *Atmospheric Chemistry and Physics*, *11*, 13,421–13,449. <https://doi.org/10.5194/acp-11-13421-2011>
- Hauer, M. E., Evans, J. M., & Mishra, D. R. (2016). Millions projected to be at risk from sea-level rise in the continental United States. *Nature Climate Change*, *6*(7), 691.
- Hobbs, W. (2016). An energy conservation analysis of ocean drift in the CMIP5 global coupled models. *Journal of Climate*, *29*, 1639–1653. <https://doi.org/10.1175/JCLI-D-15-0477>
- Hurrell, J. W., Holland, M. M., Gent, P. R., Ghan, S., Kay, J. E., Kushner, P. J., et al. (2013). The community earth system model: A framework for collaborative research. *Bulletin of the American Meteorological Society*, *94*(9), 1339–1360. <https://doi.org/10.1175/BAMS-D-12-00121.1>
- Katsman, C. A., Hazeleger, W., Drijfhout, S. S., van Oldenborgh, G. J., & Burgers, G. (2008). Climate scenarios of sea level rise for the Northeast Atlantic Ocean: A study including the effects of ocean dynamics and gravity changes induced by ice melt. *Climatic Change*, *91*, 351–374.
- Kay, J. E., Deser, C., Phillips, A., Mai, A., Hannay, C., Strand, G., et al. (2015). The community earth system model (CESM) large ensemble project: A community resource for studying climate change in the presence of internal climate variability. *Bulletin of the American Meteorological Society*, *96*(8), 1333–1349. <https://doi.org/10.1175/BAMS-D-13-00255.1>
- Kenigson, J. S., Han, W., Rajagopalan, B., Yanto, M., & Jasinski, M. (2018). Decadal shift of NAO-linked interannual sea level variability along the US northeast coast. *Journal of Climate*, *31*, 4981–4989.
- Ketabchi, H., Mahmoodzadeh, D., Ataie-Ashtiani, B., & Simmons, C. T. (2016). Sea-level rise impacts on seawater intrusion in coastal aquifers: Review and integration. *Journal of Hydrology*, *535*, 235–255.
- Kim, W. M., Yeager, S., Chang, P., & Danabasoglu, G. (2018). Low-frequency North Atlantic climate variability in the community earth system model large ensemble. *Journal of Climate*, *31*(2), 787–813.
- Knutti, R., Masson, D., & Gettelman, A. (2013). Climate model genealogy: Generation CMIP5 and how we got there. *Geophysical Research Letters*, *40*, 1194–1199. <https://doi.org/10.1002/grl.50256>
- Kopp, R. E., Horton, B. P., Kemp, A. C., & Tebaldi, C. (2015). Past and future sea-level rise along the coast of North Carolina, USA. *Climatic Change*, *132*(4), 693–707.
- Lee, S. (2014). A theory for polar amplification from a general circulation perspective. *Asia-Pacific Journal of Atmospheric Sciences*, *50*(1), 31–43.
- Lorbacher, K., Marsland, S. J., Church, J. A., Griffies, S. M., & Stammer, D. (2012). Rapid barotropic sea level rise from ice sheet melting. *Journal of Geophysical Research*, *117*, C06003. <https://doi.org/10.1029/2011JC007733>

- Lowe, J. A., & Gregory, J. M. (2006). Understanding projections of sea level rise in a Hadley Centre coupled climate model. *Journal of Geophysical Research*, *111*, C11014. <https://doi.org/10.1029/2005JC003421>
- Marshall, J., Armour, K. C., Scott, J. R., Kostov, Y., Hausmann, U., Ferreira, D., et al. (2014). The ocean's role in polar climate change: Asymmetric Arctic and Antarctic responses to greenhouse gas and ozone forcing. *Philosophical Transactions of the Royal Society A*, *372*, 20,130,040. <https://doi.org/10.1098/rsta.2013.0040>
- McDougall, T. J., Wright, D. G., Jackett, D. R., & Feistel, R. (2009). Calculation of the thermophysical properties of seawater. Global Ship-based Repeat Hydrography Manual, IOCCP Report 14.
- Merrifield, M. A. (2011). A shift in western tropical Pacific Sea level trends during the 1990s. *Journal of Climate*, *24*(15), 4126–4138. <https://doi.org/10.1175/2011JCLI3932.1>
- Meysignac, B., Boyer, T., Zhao, Z., Hakuba, M. Z., Landerer, F. W., Stammer, D., & Abraham, J. P. (2019). Measuring global ocean heat content to estimate the earth energy imbalance. *Frontiers in Marine Science*, *6*. <https://doi.org/10.3389/fmars.2019.00432>
- Milne, G. A., Gehrels, W. R., Hughes, C. W., & Tamisiea, M. E. (2009). Identifying the causes of sea-level change. *Nature Geoscience*, *2*(7), 471–478.
- Moftakhari, H. R., AghaKouchak, A., Sanders, B. F., Feldman, D. L., Sweet, W., Matthew, R. A., & Luke, A. (2015). Increased nuisance flooding along the coasts of the United States due to sea level rise: Past and future. *Geophysical Research Letters*, *42*, 9846–9852. <https://doi.org/10.1002/2015GL066072>
- Nerem, R. S., Beckley, B. D., Fasullo, J. T., Hamlington, B. D., Masters, D., & Mitchum, G. T. (2018). Climate-change-driven accelerated sea-level rise detected in the altimeter era. *Proceedings of the National Academy of Sciences*, *115*(9), 2022–2025.
- Nerem, R. S., Chambers, D. P., Choe, C., & Mitchum, G. T. (2010). Estimating mean sea level change from the TOPEX and Jason altimeter missions. *Marine Geodesy*, *33*(S1), 435–446.
- Nerem, R. S., Chambers, D. P., Leuliette, E. W., Mitchum, G. T., & Giese, B. S. (1999). Variations in global mean sea level associated with the 1997–1998 ENSO event: Implications for measuring long term sea level change. *Geophysical Research Letters*, *26*(19), 3005–3008.
- Neumann, B., Vafeidis, A. T., Zimmermann, J., & Nicholls, R. J. (2015). Future coastal population growth and exposure to sea-level rise and coastal flooding—a global assessment. *PLoS ONE*, *10*(3), e0118571. <https://doi.org/10.1371/journal.pone.0118571>
- Previdi, M., & Polvani, L. M. (2014). Climate system response to stratospheric ozone depletion and recovery. *Quarterly Journal of the Royal Meteorological Society*, *140*(685), 2401–2419.
- Royston, S., Watson, C. S., Legresy, B., King, M. A., Church, J. A., & Bos, M. S. (2018). Sea-level trend uncertainty with Pacific climatic variability and temporally-correlated noise. *Journal of Geophysical Research: Oceans*, *123*, 1978–1993. <https://doi.org/10.1002/2017JC013655>
- Slangen, A. B., Church, J. A., Zhang, X., & Monselesan, D. P. (2015). The sea level response to external forcings in historical simulations of CMIP5 climate models. *Journal of Climate*, *28*, 8521–8539.
- Smith, D. M., Allan, R. P., Coward, A. C., Eade, R., Hyder, P., Liu, C., et al. (2015). Earth's energy imbalance since 1960 in observations and CMIP5 models. *Geophysical Research Letters*, *42*, 1205–1213. <https://doi.org/10.1002/2014GL062669>
- Stammer, D. (2008). Response of the global ocean to Greenland and Antarctic ice melting. *Journal of Geophysical Research*, *113*, C06022. <https://doi.org/10.1029/2006JC004079>
- Swart, N. C., & Fyfe, J. C. (2012). Observed and simulated changes in the Southern Hemisphere surface westerly wind-stress. *Geophysical Research Letters*, *39*, L16711. <https://doi.org/10.1029/2012GL052810>
- Tebaldi, C., & Arblaster, J. M. (2014). Pattern scaling: Its strengths and limitations, and an update on the latest model simulations. *Climatic Change*, *122*(3), 459–471.
- Thompson, P. R., Hamlington, B. D., Landerer, F. W., & Adhikari, S. (2016). Are long tide gauge records in the wrong place to measure global mean sea level rise? *Geophysical Research Letters*, *43*, 10,403–10,411. <https://doi.org/10.1002/2016GL070552>
- Tokarska, K. B., Hegerl, G. C., Schurer, A. P., Ribes, A., & Fasullo, J. T. (2019). Quantifying human contributions to past and future ocean warming and thermocline sea level rise. *Environmental Research Letters*, *14*(7), 074020.